

# Effectiveness of TeV $\gamma$ -ray observations at large zenith angles with a stereoscopic system of imaging atmospheric Čerenkov telescopes

A. Konopelko, F. Aharonian, M. Hemberger, W. Hofmann,  
J. Kettler, G. Pühlhofer, H.J. Völk

Max-Planck-Institut für Kernphysik, D-69029 Heidelberg, Germany

**Abstract.** The sensitivity of imaging atmospheric Čerenkov telescopes (IACTs) in TeV  $\gamma$ -ray observations reaches its maximum at small zenith angles ( $\Theta \leq 30^\circ$ ) which provide the minimum attainable energy threshold of an instrument. However, for a specific telescope site a number of  $\gamma$ -ray sources, or source candidates, can only be observed at much larger zenith angles ( $\Theta \leq 60^\circ$ ). Moreover the observations at large zenith angles allow to extend the observation time window for any object seen at small zenith angles, as well as to enlarge the dynamic energy range of an instrument towards the highest observable energies of  $\gamma$ -rays. Based on Monte Carlo simulations we present here the results on the sensitivity of a stereoscopic system of 5 IACTs in observations at large zenith angles. We point out some important parameters of the telescope design which could substantially improve the efficiency of such observations with forthcoming IACT arrays like CANGAROO III, HESS and VERITAS.

## 1. Introduction

Ground-based very high energy (VHE)  $\gamma$ -ray astronomy explores the energy range from 200 GeV up to 20 TeV. Recent exciting detections and observations of a number of  $\gamma$ -ray sources have demonstrated the very high sensitivity of the imaging atmospheric Čerenkov technique (Weekes et al. 1997; Ong, 1998). The performance of this technique appears to be strongly dependent on the zenith angle range covered while tracking an object. The accessible zenith angle range is simply determined by the latitude of the detector and the celestial coordinates of a particular object. The  $\gamma$ -ray observations are likely to be made up to zenith angles  $30^\circ$  in order to detect high quality two-dimensional angular *images* of Čerenkov light from air showers. Extension of observations to larger zenith angles (up to  $60^\circ$ ) might substantially widen the observational time window for a number of objects. Apparently that is very important for multiwavelength campaigns involving ground-based and satellite-born instruments in simultaneous observations of variable  $\gamma$ -ray sources, e.g. BL Lac objects. In addition observations at large zenith angles favour the detection of the high energy  $\gamma$ -rays,  $E \geq 10$  TeV, which, at present, can be registered only using the ground-based Čerenkov technique, and set important constraints on  $\gamma$ -ray emission mechanisms.

Sommers & Elbert (1987) first noticed that the effective detection area for  $\gamma$ -ray air showers dramatically increases in observations at large zenith angles using Čerenkov detectors. Expedient use of large zenith angle observations using imaging Čerenkov technique was suggested in the proposal of the HEGRA IACT array (Aharonian et al., 1989). Hillas & Patterson (1991) made first simulations of Čerenkov light images from air showers with an inclination of  $60^\circ$ . The Whipple group has developed the analysis technique for a single stand-alone 10 m telescope (see e.g. Krennrich et al. 1999) and tested it by observations of Mkn 421 and Mkn 501. Large zenith angle observations have been used with the 3.8 m Čerenkov telescope operated by the CANGAROO group (Tanimori et al., 1998) to measure the energy spectrum of the Crab Nebula up to  $\simeq 50$  TeV. Here we present results from Monte Carlo simulations of inclined air showers (zenith angle of  $60^\circ$ ) for a *stereoscopic system* of five imaging air Čerenkov telescopes (IACTs). We discuss the major change in topology of Čerenkov light emission from air showers at large inclinations, which determines the detection rates as well as the ability to classify images of  $\gamma$ -rays. We have compared the sensitivity of the IACT system at small ( $20^\circ$ ) (SZA) and large ( $60^\circ$ ) (LZA) zenith angles. Current observations with the HEGRA IACT system generally confirm the Monte Carlo predictions (these results will be published elsewhere).

## 2. Air shower simulations

The ALTAI Monte Carlo code (Konopelko et al. 1996; 1999) was used to generate  $\gamma$ -ray and cosmic ray induced air showers. This code includes a detailed model of Rayleigh (molecular) scattering, aerosol (Mie) scattering and ozone absorption of Čerenkov

light in the atmosphere (Elterman, 1968; Driscoll, Vaughan, 1978). This model has been checked against the available experimental data for La Palma, Canary Islands (Hemberger, 1998). The calculations have been done with allowance for the effect of the geomagnetic field. By additional test simulations we found that the effect of multiple-scattering of Čerenkov light photons in the atmosphere is negligible because of a low aerosol content above the observation level (2.2 km above sea level) as well as due to the specific shape of the aerosol scattering-phase function (Driscoll, Vaughan, 1978) for SZA as well as for LZA.

Simulations were performed for the setup of five IACTs of the HEGRA stereoscopic system (Aharonian et al. 1999). Each of five telescopes consists of a 8.5 m<sup>2</sup> reflector focussing onto a photomultiplier tube camera. The number of photomultipliers in the camera was 271, arranged in a hexagonal matrix covering a field of view with a diameter of 4.3°. A telescope camera was triggered when the signal in two of the 271 photomultiplier tubes exceeded a threshold of 8 photoelectrons, and the event was saved when at least two telescopes were triggered by Čerenkov light from air shower. The overall efficiency of the photon-to-photoelectron conversion was about 0.1.

### 3. Lateral distribution of Čerenkov light photons

The longitudinal profile of the number of secondary electrons in air showers of a fixed primary energy,  $E$ , remains almost the same at different shower inclinations when the distance along the shower axis is measured in  $\text{gr}/\text{cm}^2$ . The depth of shower maximum can be calculated as  $T_{\text{max}} = X_0 \cdot \ln(E/E_c)$  ( $X_0$  and  $E_c$  are the radiation length and critical energy in air, respectively) (e.g., Nishimura, 1967). Thus a 3 TeV  $\gamma$ -ray air shower at zenith has, on average, a maximum in electron number at a depth of  $T_{\text{max}} \simeq 400 \text{ gr}/\text{cm}^2$ , which corresponds to  $H_{\text{max}} \simeq 7.5 \text{ km}$  above the sea. For large inclinations the total atmospheric optical depth increases substantially and the shower develops entirely in the upper layers of the atmosphere. For air showers with large inclinations, the height of shower maximum is far above the observation level, and the geometrical distance from the shower maximum to the observer is correspondingly very large. Thus a  $\gamma$ -ray-induced air shower of 3 TeV with 60° inclination on average has an electron maximum at  $H_{\text{max}} \simeq 12 \text{ km}$  above the observation level. The corresponding geometrical distance from the shower maximum to observer,  $L_{\text{max}}$ , for such a shower is about 24 km. These geometrical factors determine the distribution of Čerenkov light in the plane perpendicular to the shower core. Air showers at the zenith give a high Čerenkov photon density in the region close to the shower core ( $R \leq 100 \text{ m}$ ) (see Figure 1) because of high photon emission from the low energy electrons ( $E_e \leq 1 \text{ GeV}$ ) which deeply penetrate into the atmosphere and suffer multiple Coulomb scattering. In air showers with large inclinations these electrons contribute over a much wider range of distances from the shower core because of the larger geometrical distance to the shower maximum, and as a result the corresponding mean photon density is substantially lower. In addition, the absorption of Čerenkov light photons in the atmosphere increases for

**Table 1.** Detection rates of  $\gamma$ -ray and cosmic ray-induced air showers for inclination of  $20^\circ$  and  $60^\circ$  and corresponding signal to noise ratio for all triggered events and for the high energy events above 20 TeV.

	Zenith angle:	$20^\circ$	$60^\circ$
All events	$R_\gamma$ , [hr $^{-1}$ ]	100	43
	$R_{CR}$ , [hr $^{-1}$ ]	$5.4 \cdot 10^4$	$2.7 \cdot 10^4$
	S/N, $\sigma$	0.3	0.18
$E \geq 20$ TeV	$R_\gamma$ , [hr $^{-1}$ ]	1.2	5
	$R_{CR}$ , [hr $^{-1}$ ]	$8 \cdot 10^2$	$1.6 \cdot 10^3$
	S/N, $\sigma$	0.03	0.09

air showers with large inclinations due to the large optical depth on the way from the point of their emission to the detector.

The characteristic hump in the lateral distribution of Čerenkov light photons, caused by the emission of energetic electrons ( $E_e \geq 1$  GeV) around the shower maximum, is shifted to larger distances from the shower axis. One can estimate the position of the hump using the expression  $R_0 \sim L_{\max} \cdot \text{tg}\theta_c$ , where  $\theta_c = \theta_c(H_{\max})$  is the Čerenkov light emission angle at the corresponding shower maximum height,  $H_{\max}$ . Thus for a 3 TeV  $\gamma$ -ray shower at the zenith and for  $60^\circ$  inclination the offset of the hump is 90 and 240 m, respectively. These “toy model” estimates are in good agreement with the simulations (see Figure 1). The hump becomes even more prominent at  $60^\circ$  inclination because of the reduced density of Čerenkov light photons emitted by low energy electrons.

#### 4. Collection areas and detection rates

Despite the sophisticated trigger logics, the trigger condition for each telescope of a system ultimately relies on the size of the image (i.e., total number of ph.-e.) in the camera. Thus the trigger efficiency for each telescope, as well as for the entire system roughly reflects the lateral distribution of Čerenkov light photons at the observation level. Finally, the effective collection area is governed by the lateral distribution of Čerenkov light photons (for details see Aharonian et al., 1995). Results of calculations for a 5 IACT system are shown in Figure 2. A sharp increase in collection areas at low energies, caused by increasing trigger efficiency within the plateau of Čerenkov light density ( $R \geq 130$  m), changes above  $S_\gamma \sim 5 \cdot 10^4 \text{ m}^2$  to a logarithmic growth at the exponential tail of the Čerenkov light lateral distribution (see Figure 1). At large inclinations low energy  $\gamma$ -rays ( $E \leq 1$  TeV) cannot trigger the telescope system because of the very low average image size. At the same time the broad lateral distribution for high energy  $\gamma$ -rays ( $E \geq 3$  TeV) provides large collection areas which could even substantially exceed the collection areas at small zenith angles (see Figure 2). Thus, for 10 TeV the  $\gamma$ -ray collection area for LZA is larger by a factor of 3.5 than for SZA.

Assuming an energy spectrum of  $\gamma$ -rays, e.g.,  $dJ_\gamma/dE \propto E^{-\alpha}$ ;  $\alpha = 2.5$ , and a certain flux normalization,  $J_\gamma(> 1 \text{ TeV}) = 10^{-11} \text{ cm}^{-2}\text{s}^{-1}$ , one can calculate the detection rates

**Table 2.** Effective energy threshold of  $\gamma$ -ray induced air showers at different inclination angles.

$\Theta$ , deg	0	20	30	45	60
$E_{\text{th}}$ , TeV	0.5	0.7	0.9	1.8	5.0

of  $\gamma$ -ray-induced air showers

$$R_{\gamma}(> E_o) = \int_{E_o} S_{\gamma}(E) \frac{dJ_{\gamma}}{dE} dE \quad (1)$$

and cosmic ray showers

$$R_{CR}(> E_o) = \int_{\Omega_o} d\Omega \int_{E_o} S_{CR}(E, \Omega) \frac{dJ_{CR}}{dE} dE \quad (2)$$

above the energy threshold of  $E_o$ , where  $\Omega_o$  is the solid angle of the isotropic cosmic ray air showers, and  $S_{\gamma}$  and  $S_{CR}$  are the collection areas for  $\gamma$ -rays and cosmic rays, respectively.  $E$  is a reconstructed energy of  $\gamma$ -ray and cosmic ray induced air showers using the procedure tuned for the  $\gamma$ -rays (see Konopelko et al, 1999). The integral detection rates calculated for SZA and LZA are shown in Figure 3. Note that for  $\gamma$ -rays above 20 TeV the integral detection rate is about 4 times higher for LZA than for SZA, whereas the corresponding integral cosmic ray rate is higher by a factor of 2, only. Thus at the trigger level LZA observations reveal a substantial advantage in the detection rate of high energy  $\gamma$ -rays as well as a high signal to noise ratio,  $S/N = R_{\gamma}/(2 \cdot R_{CR})^{1/2}$  (see Table 1) ‡ The signal to noise ratio for the high energy events (above 20 TeV) strongly depends on the energy spectrum index of  $\gamma$ -rays. In case of a flat energy spectrum ( $\alpha \sim 2.0$ ) the advantage at LZA becomes even more prominent (see below). The effective energy threshold of the telescope system, defined as the energy at which  $\gamma$ -ray detection rate reaches its maximum for the differential energy spectrum  $dN_{\gamma}/dE \sim E^{-2.5}$ , is  $\sim 0.5$  TeV at zenith, and increases at larger inclinations (see Table 2).

## 5. Orientation and shape of Čerenkov light images

The above mentioned features of the shower development at large inclinations determine the topology of Čerenkov light images. We show in Figure 4 Čerenkov light images calculated for 3 TeV  $\gamma$ -ray-induced air shower with various inclinations. In general the images at large inclinations (a) contain less photons; (b) become smaller in size; (c) shrink to the camera center; and, (d) have a circular shape. Using our “toy model” considerations we may estimate the position of the image centroid (maximum of image

‡ In TeV  $\gamma$ -ray observations the significance of  $\gamma$ -ray signal is calculated as  $S/N = \text{ON} - \text{OFF}/(\text{ON} + \text{OFF})^{1/2}$  where ON is the number of events registered while tracking the source and OFF is the corresponding number of background events,  $N_{CR}$ .  $\text{ON} - \text{OFF}$  gives the number of detected  $\gamma$ -ray showers,  $N_{\gamma}$ . In the case when  $\text{OFF} \gg \text{ON} - \text{OFF}$  one can modify the formulae as follows:  $N_{\gamma}/(2 \cdot N_{CR})^{1/2} = R_{\gamma}/(2 \cdot R_{CR})^{1/2} \cdot \sqrt{t}$ , where  $t$  is the observational time and  $R_{\gamma}, R_{CR}$  are the rates of  $\gamma$ -rays and cosmic rays, respectively.

**Table 3.** Acceptances of  $\gamma$ -ray showers after angular cut for two inclinations,  $20^\circ$  and  $60^\circ$ .  $\theta$  is the angular distance from the reconstructed to the actual  $\gamma$ -ray source position.

Zenith angle:	$20^\circ$	$60^\circ$
$\theta \leq 0.3^\circ$	0.90	0.52
$\theta \leq 0.55^\circ$	0.95	0.70

**Table 4.** Acceptances of  $\gamma$ -ray and cosmic ray showers and corresponding enhancement (Q-factor) after applying mean scaled Width cut. Air showers were simulated at two inclinations,  $\theta = 20^\circ$  and  $60^\circ$ .

	Cut:	$\kappa_\gamma$	$\kappa_{cr}$	Q-factor
$\theta = 20^\circ$	$\langle \tilde{w} \rangle \leq 1.0$	0.53	0.01	5.3
	$\langle \tilde{w} \rangle \leq 1.3$	0.99	0.15	2.6
$\theta = 60^\circ$	$\langle \tilde{w} \rangle \leq 1.0$	0.45	0.05	2.0
	$\langle \tilde{w} \rangle \leq 1.3$	0.90	0.30	1.6

intensity set by the emission from shower maximum) in a telescope focal plane as  $\theta_0 \sim 1/\text{tg}(R_0/L_{\text{max}})$ . At 100 m impact distance from the shower axis the centroid position is at  $\simeq 1^\circ$  and  $\simeq 0.23^\circ$ , for air showers at the zenith and for  $60^\circ$  inclination, respectively. The small angular size of Čerenkov light images at large inclinations was noticed by Hillas & Patterson (1990). Air showers with  $60^\circ$  inclination are very far from the observer which is why the image angular size is getting small in both longitudinal and transverse directions. The lateral spread of electrons ( $\rho_o$ ) in the maximum of multi-TeV  $\gamma$ -ray shower is  $\sim 20$  m (see e.g., Hillas, 1996). Thus the angular size of the Čerenkov light image along the minor image axis can be estimated as  $w \sim 1/\text{tg}(R_0/L_{\text{max}}) - 1/\text{tg}((R_0 - \rho_o)/L_{\text{max}})$ . It is of  $\simeq 0.2^\circ$  for shower at zenith and  $\simeq 0.06^\circ$  for the shower with  $60^\circ$  inclination (see Figure 4). To measure the orientation and shape of these images one needs a relatively small pixel size (angular size of PMTs in camera)  $\sim 0.1 \div 0.15^\circ$ . Note also that light smearing by optical errors may significantly distort the angular shape of these images. The ratio of standard second moment parameters,  $Width/Length$ , shifts to larger values (see Figure 6) for showers at large inclinations. It shows that these images have a circular shape rather than an elongated elliptic shape. Consequently the image orientation is determined with larger uncertainties.

For the image orientation one can use the standard *Alpha*-parameter which defines the angle between the major axis of an elliptical image and the line connecting the position of the image maximum to the camera center (we assume that telescopes are looking directly onto the source of  $\gamma$ -rays). The distribution of *Alpha*-parameter for all triggered telescopes in a system observing the  $\gamma$ -rays at  $20^\circ$  and  $60^\circ$  inclination is shown in Figure 5. The distribution at large inclination is relatively broader as expected. This

implies that  $\gamma$ -ray acceptance after applying the angular cut is less at large inclinations (see Table 3) and the corresponding enhancement factor is lower. Note that an imaging camera with small pixels ( $\sim 0.1 \div 0.15^\circ$ ) may substantially improve the angular resolution at large inclinations.

In order to utilize simultaneously several Čerenkov light images for an individual shower the so-called *mean scaled Width* parameter (Konopelko, 1995; Daum et al., 1996) can be effectively used for a system of IACTs. To compensate the dependence of the image shape on primary shower energy and distance from shower core to the telescope (impact parameter) the standard parameter *Width* (see Fegan, 1997) ( $w^k$ ), calculated for each telescope, is scaled according to the Monte Carlo predicted values,  $\langle w \rangle_{ij}^k$ , taken for the corresponding bin of reconstructed distance from the telescope to the shower core (i) and for the corresponding bin of image size (total number of photoelectrons in the image)(j). The *mean scaled Width* parameter is defined for each individual shower as follows

$$\langle \tilde{w} \rangle = 1/N \sum_{k=1}^N w^k / \langle w \rangle_{ij}^k \quad (3)$$

where  $N$  is the number of triggered telescopes. The optimum cut on mean scaled Width is about 1.0, which gives a  $\gamma$ -ray acceptance of  $\sim 50\%$ . However, for a precise determination of  $\gamma$ -ray spectra, a loose cut on mean scaled width ( $\langle \tilde{w} \rangle < 1.2$ ) has been so far used in data analysis (Aharonian et al, 1999) in order to maximize the  $\gamma$ -ray acceptance and to minimize systematic error related to cut efficiencies. In Table 4 we show the acceptances and efficiencies of a  $\gamma$ -ray classification using the *mean scaled Width* cut. The small angular size of both  $\gamma$ -ray and cosmic ray induced air showers prevents effective rejection using  $\langle \tilde{w} \rangle$ -parameter for LZA. The resulting enhancement (Q-factor) does not exceed 2.0 whereas at small zenith angle it is more than 5.0. We may conclude that the standard orientation and shape cuts, usually used for the IACT system analysis, allow less significant rejection of the cosmic rays. In order to improve the cosmic ray rejection we introduced an additional parameter, *mean scaled Length*,  $\langle \tilde{l} \rangle$ , defined by analogy with  $\langle \tilde{w} \rangle$ . Two parameters,  $\langle \tilde{w} \rangle$  and  $\langle \tilde{l} \rangle$ , can be used for calculating a Mahalanobis distance, MD (see Mahalanobis, 1963), in 2-dimensional space

$$\text{MD} = ((1 - \langle \tilde{w} \rangle)^2 / \sigma_{\langle \tilde{w} \rangle}^2 + (1 - \langle \tilde{l} \rangle)^2 / \sigma_{\langle \tilde{l} \rangle}^2)^{1/2} \quad (4)$$

where  $\sigma_{\langle \tilde{w} \rangle}$  and  $\sigma_{\langle \tilde{l} \rangle}$  are standard deviations for the corresponding distributions of  $\langle \tilde{w} \rangle$  and  $\langle \tilde{l} \rangle$ . We found that the optimum value for the MD cut for LZA is 1.5. This analysis improves the enhancement factor by  $\simeq 30\%$ . Note that multivariate analysis technique for a single Čerenkov telescope has been discussed before by Aharonian et al. (1991); Hillas & West (1991). In addition we have applied the standard algorithms of the impact distance and energy reconstruction (e.g., Konopelko et al., 1999) used for the system of 5 IACTs to events simulated at large inclinations. A summary of a system performance at LZA is presented in Table 5.

## 6. Sensitivity to $\gamma$ -ray fluxes

The sensitivity of the instrument can be characterized using the so-called *sigma-per-hour* parameter. It corresponds to the signal to noise ratio which one can achieve within one hour observations of  $\gamma$ -ray source assuming a certain DC  $\gamma$ -ray flux, e.g.,  $J_\gamma(\geq 1 \text{ TeV}) = 10^{-11}$  [photons/cm<sup>2</sup>s] and the energy spectrum  $dJ_\gamma/E \propto E^{-2.5}$ . Thus the sensitivity of the 5 IACT system is about  $6\sigma$  and  $\sim 1\sigma$  (loose cuts) at the small ( $20^\circ$ ) and large ( $60^\circ$ ) zenith angles. These sensitivities can be explained by the difference in the energy threshold and  $\gamma$ -ray rate for LZA and SZA. Thus, for a proper comparison of system performance one can use a “sigma-per-hour” for energy bin,  $\sigma/hr/\log(E)$ . This parameter corresponds to the signal to noise ratio which one could expect detecting  $\gamma$ -rays in a fixed energy range. In present analysis we choose the corresponding energy bin as  $\Delta E_i = E_{i+1} - E_i$ ,  $E_{i+1}/E_i = 1.38$  which roughly corresponds to the energy resolution at LZA. The number of  $\gamma$ -ray and cosmic ray induced showers detected within the energy bin  $\Delta E_i$  can be calculated as

$$N_i^\gamma = \int_{E_i}^{E_{i+1}} \left( \frac{dR^\gamma}{dE} \right) \cdot dE, \quad N_i^{\text{CR}} = \int_{E_i}^{E_{i+1}} \left( \frac{dR^{\text{CR}}}{dE} \right) \cdot dE, \quad (5)$$

and the corresponding signal to noise ratio is

$$S_i = N_i^\gamma / (2 \cdot N_i^{\text{CR}})^{1/2}. \quad (6)$$

where  $(dR^\gamma/dE)$  and  $(dR^{\text{CR}}/dE)$  are the differential detection rates of  $\gamma$ -ray and cosmic ray air showers.

The  $\sigma/hr/\log(E)$  as a function of primary  $\gamma$ -ray energy,  $S = S(E)$ , is shown in Figure 7. Our calculations demonstrate that for a  $\gamma$ -ray source with a spectrum index of 2.5, LZA observations have an advantage at trigger level before imaging analysis. After applying the software analysis cuts, the sensitivity is almost the same at 10 TeV with a slight advantage for LZA for higher energies. For flat-spectrum  $\gamma$ -ray sources ( $\alpha \sim 2.0$ ) the signal-to-noise ratio is a factor of 3 higher at  $\sim 20$  TeV for LZA compared with SZA. For the data shown in Figure 7 we have applied the *loose* analysis cuts. These cuts keep most of the  $\gamma$ -rays ( $\kappa_\gamma \simeq 0.9$ ), which is preferable for the spectrum studies. However these cuts give only a modest cosmic ray background rejection with the corresponding quality factor of  $\simeq 12$  for SZA and  $\simeq 5$  for the LZA. Note that in order to achieve the maximum signal-to-noise ratio one can use the *tight* cuts ( $\theta \leq 0.22^\circ$ ,  $\langle \tilde{w} \rangle < 1.0$ ) which provide a  $\gamma$ -ray acceptance of  $\kappa_\gamma \simeq 0.4$  and corresponding Q-factors as high as  $\simeq 35$  and  $\sim 10$  for SZA and LZA, respectively.

## 7. Conclusions

We have studied the efficiency of large zenith angle observations using the stereoscopic system of 5 imaging atmospheric Čerenkov telescopes by means of detailed Monte Carlo simulations. LZA observations give a very large effective collection area at large zenith angles but a modest ability for  $\gamma$ -ray classification. The results of simulations show that



**Table 5.** Accuracy of determination of impact distance ( $\Delta R$ ), angular resolution ( $\delta\Theta$ ), and energy resolution ( $\Delta E/E$ ), for a system of 5 IACTs.

Zenith angle:	20°	60°
$\Delta R$ , m	$\leq 10$	$\leq 50$
$\delta\Theta$ , degree	0.1	0.3
$\Delta E/E$ , %	20	$\leq 30$

for a  $\gamma$ -ray source with a relatively steep energy spectrum ( $\alpha \geq 2.5$ ) LZA observations provide almost the same sensitivity as normal SZA observations at the energy of  $\gamma$ -rays of about 10 TeV with some advantage at higher energies. For  $\gamma$ -ray sources with a flat energy spectrum ( $\alpha_\gamma \sim 2.0$ ) LZA observations have a significantly higher sensitivity at energies  $\geq 10$  TeV.

Observations at large zenith angles with the forthcoming arrays of imaging atmospheric Čerenkov telescopes, like CANGAROO III, HESS and VERITAS, with an energy threshold of 50-100 GeV, could provide an extension of dynamic energy range up to 20-50 TeV. Such observations would need a camera with small pixel size of  $\sim 0.1 \div 0.15^\circ$  and fine optics of the telescope reflector.

## 8. References

- Aharonian, F., et al., 1989 *Proposal for Imaging Air Čerenkov Telescopes in the HEGRA Particle Array*
- Aharonian, F., et al., 1991 *NIM in Phys. Res.* **A302** 522-528
- Aharonian, F., et al., 1995 *J. Phys. G: Nucl. Part. Phys.* **21** 419-428
- Aharonian, F., et al., 1999 *Astron. Astrophys.* **342** 69-86
- Daum, A., et al, 1998, *Astroparticle Physics*, Vol. 8, Nos. 1-2, p. 1
- Driscoll, W., Vaughan, W. 1978 *Handbook of optics* MCGRAW-HILL book company
- Elterman, L. 1968 *AFCLR-68-0153*, Bedford, Massachusetts
- Fegan, D. 1998, *J. Phys. G: Nucl. Part. Phys.* **23**, 1013
- Hemberger, M. 1998 *PhD thesis*, Heidelberg
- Hillas, A.M., Patterson, J. 1990 *J. Phys. G: Nucl. Part. Phys.* **16** 1271-1281
- Hillas, A.M., 1996 *Space Science Reviews*, vol. 75, N 1-2, 17
- Hillas, A.M., West, A. 1991 *Proc. 22nd ICRC*, Dublin, 1, 472
- Konopelko, A., 1995, in *Proc. Towards a Major Atmospheric Čerenkov Detector-IV*, Padova (ed. by M. Cresti), p. 373
- Konopelko, A., et al. (HEGRA Collaboration) 1996, *Astroparticle Physics*, **4**, 199
- Konopelko, A., et al. (HEGRA Collaboration) 1999, *Astroparticle Physics*, **10**, 275
- Krennrich, F., et al., 1999, *ApJ* **511**, 149
- Nishimura, J. 1967, *Nandbuch der Physik* XLVI/2, 1
- Ong, R. 1998, *Physics Reports*, **305**, 3-4, 94
- Sommers, P., Elbert, J. 1987 *J. Phys. G: Nucl. Phys.* **13** 553-566
- Tanimori T., et al., 1998 *ApJ* **492** L33-L36

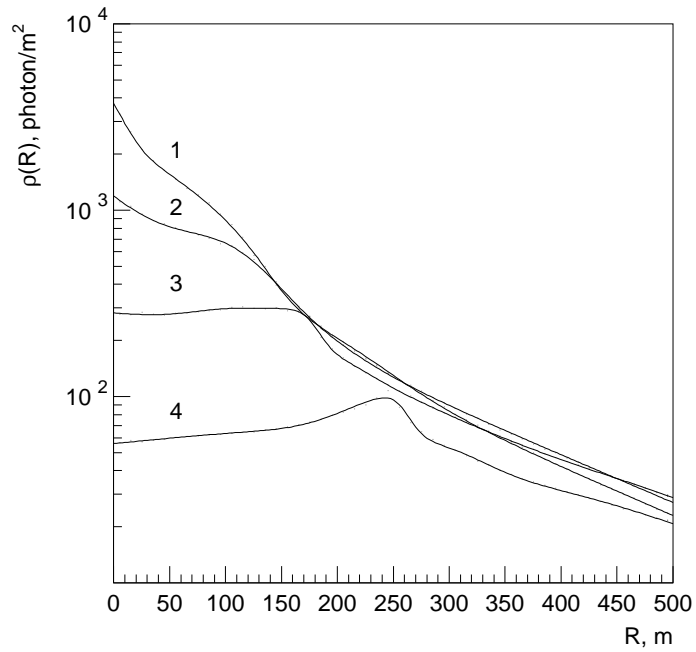


**Figure 1.** Lateral distribution of Čerenkov light density in 3 TeV  $\gamma$ -ray-induced air shower with inclination angle of 0°(1); 30°(2); 45°(3) and 60°(4). The observation level is about 2.2 km above the sea.

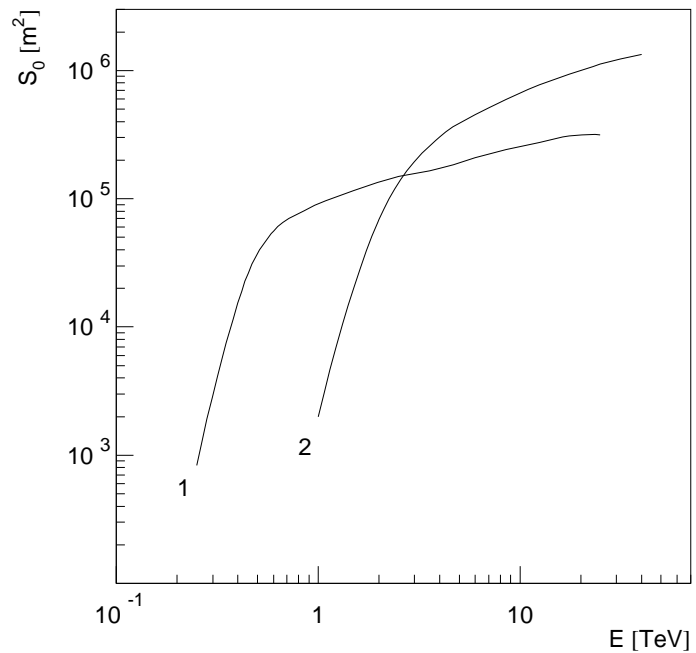


**Figure 2.** Detection area as a function of a primary shower energy for  $\gamma$ -ray-induced air showers with inclination angle of 20°(1) and 60°(2).

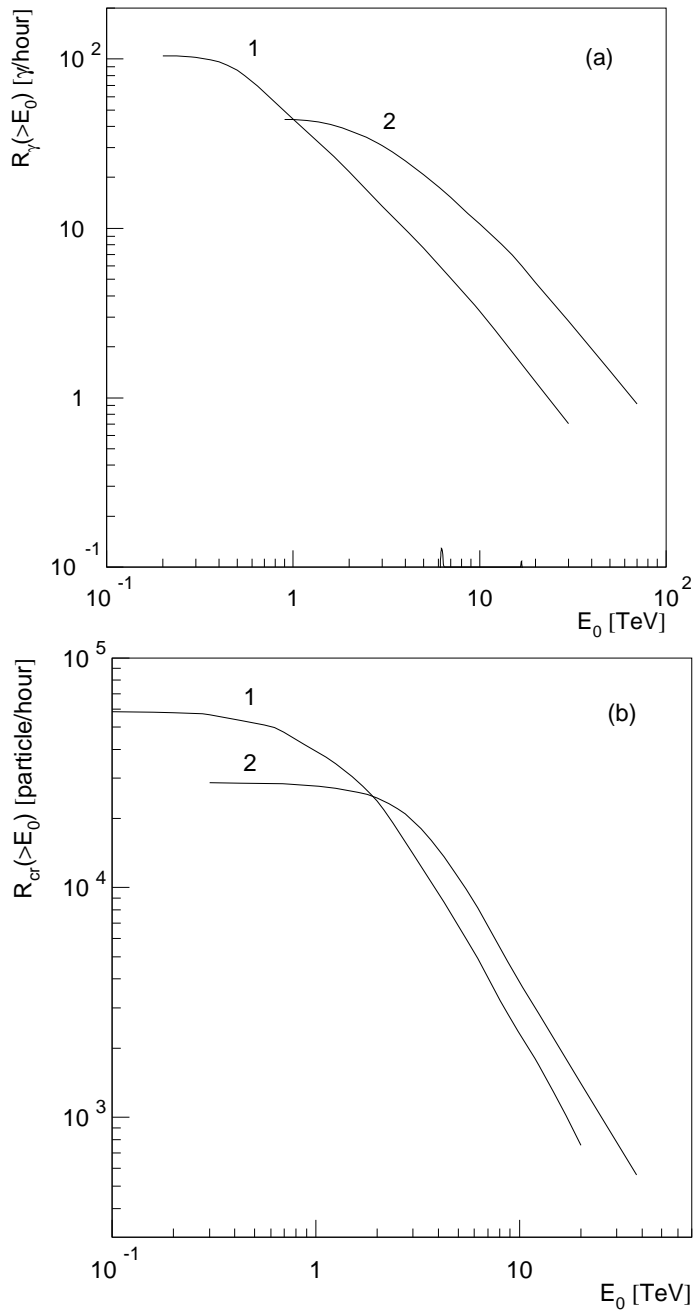


**Figure 3.** Integral detection rates of  $\gamma$ -ray (a) and cosmic ray (b) air showers above the energy  $E_0$  for two inclination angles,  $20^\circ$ (1) and  $60^\circ$ (2).

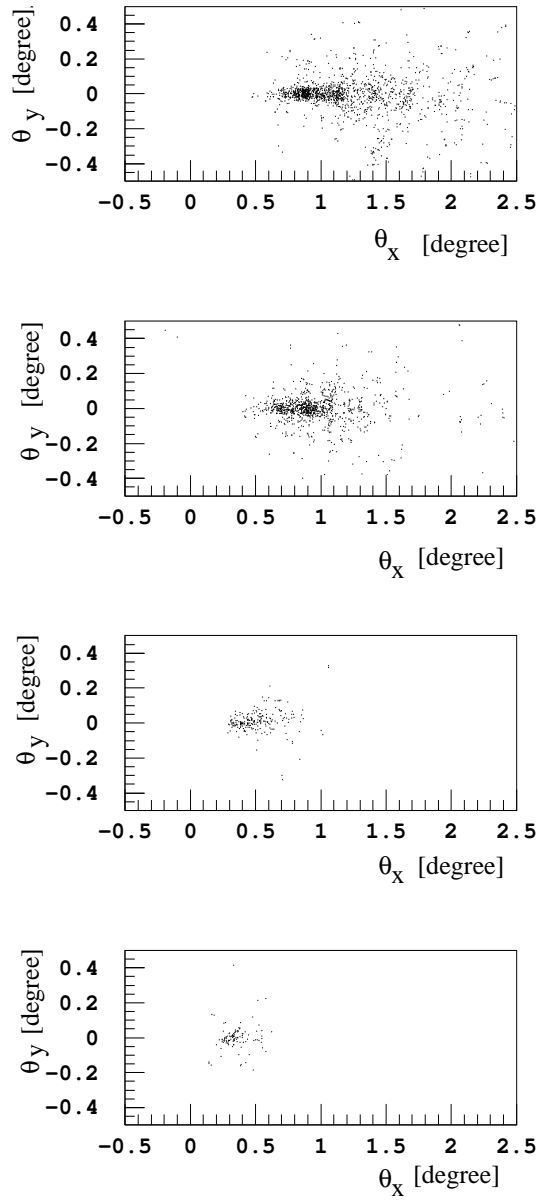


**Figure 4.** Čerenkov light images of 3 TeV  $\gamma$ -ray air shower simulated at different inclination angles,  $0^\circ$ ,  $30^\circ$ ,  $45^\circ$  and  $60^\circ$  (from upper to bottom panel). The calculated images reproduce the two-dimensional angular distributions  $(\theta_x, \theta_y)$  of Čerenkov light photons hitting the telescope reflector. Angle  $\theta_x$  is measured respecting the axis which connects the telescope mirror and the shower core. The impact distance from the shower core to the telescope is about 100 m.

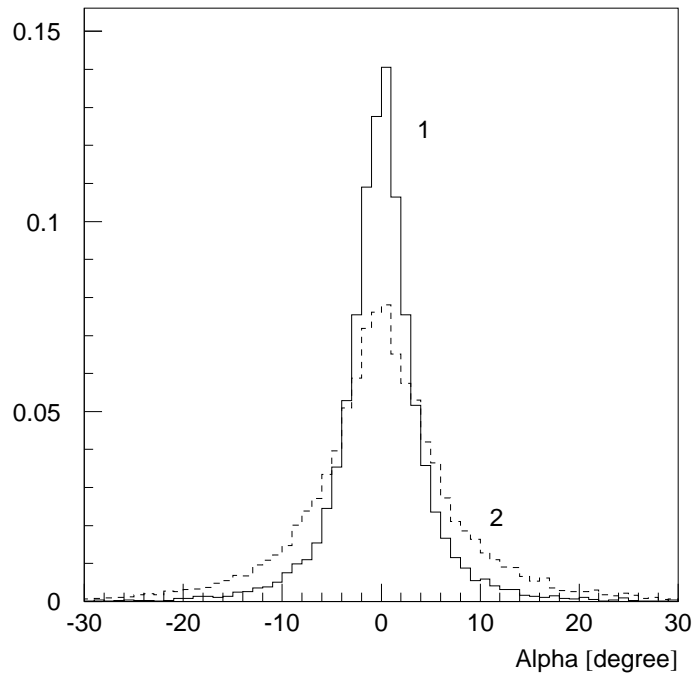


**Figure 5.** Distribution of image orientation parameter  $Alpha$  for  $\gamma$ -ray-induced air showers simulated at inclination angles of  $20^\circ$ (1) and  $60^\circ$ (2).

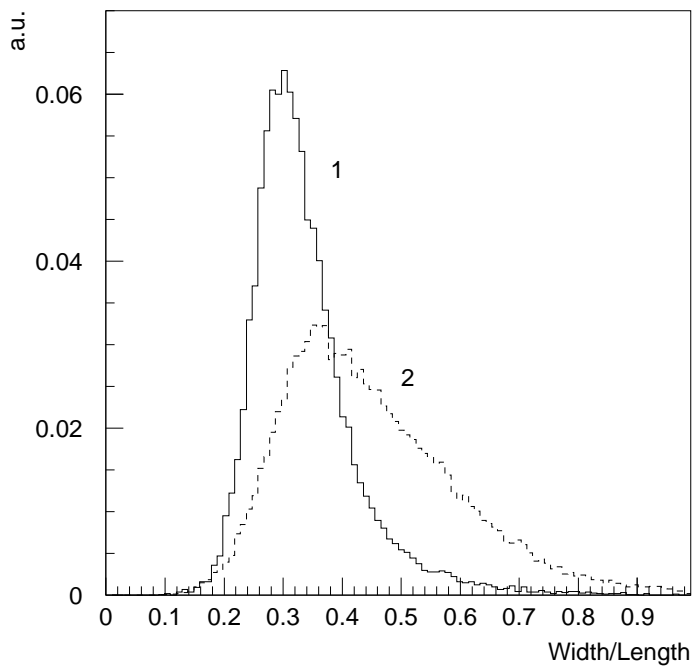


**Figure 6.** Distribution of  $Width/Length$  ratio for  $\gamma$ -ray-induced air showers simulated for the inclination angle of  $20^\circ$ (1) and  $60^\circ$ (2).

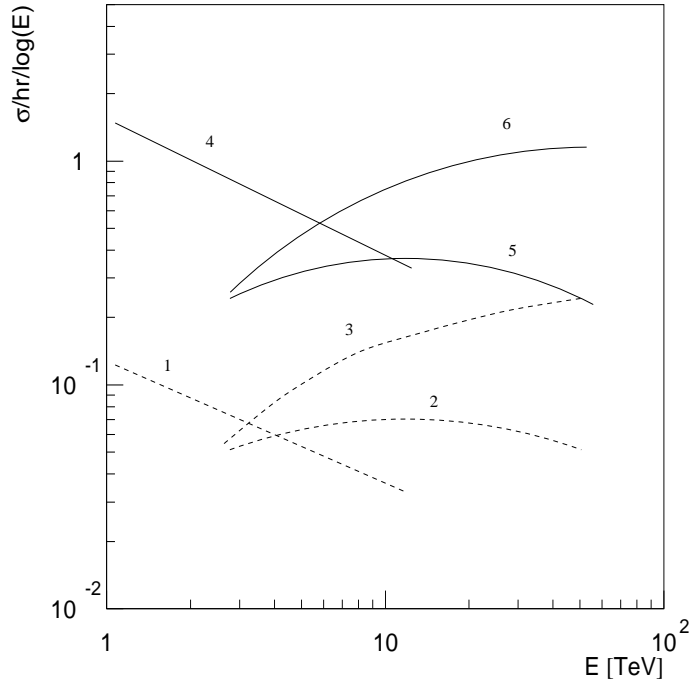


**Figure 7.** Expected signal-to-noise ratio (see eqn. 5) in observations at small zenith angles ( $20^\circ$ ) before (curve 1) and after (curve 4) *lose* analysis cuts, assuming the differential energy spectrum  $dJ_\gamma/dE \sim E^\alpha, \alpha = 2.5$  with normalization  $J_\gamma(> 1 \text{ TeV}) = 10^{-11} \text{ cm}^{-2}\text{s}^{-1}$  as well as for the large zenith angles ( $60^\circ$ ), before (2,  $\alpha = 2.5$ ; 3,  $\alpha = 2.0$ ) and after software cuts (5,  $\alpha = 2.5$ ; 6,  $\alpha = 2.0$ ).